Low carbon steel CCT diagram prediction using machine learning

A. G. Zinyagin, *Cand. Eng., Associate Prof.* [1]*, e-mail: ziniagin_ag@bmstu.ru;*
D. A. Brayko, *Postgraduate Student* [1]*, e-mail: brayko@bmstu.ru;*
A. V. Muntin, *Cand. Eng., Associate Prof.* [1]*, e-mail: muntin_av@bmstu.ru;*
P. Yu. Zhikharev, *Senior Lecturer* [1]*, e-mail: zhikharev@bmstu.ru*

[1] *Bauman Moscow State Technical University (Moscow, Russia)*

This paper presents an approach to predicting Continuous Cooling Transformation (CCT) diagrams of low-carbon steels using a mathematical model based on regression and classification. The method of digitizing CCT diagrams and its application taken from atlases and current scientific articles are given. The digitization method is based on reading the color value from the CCT diagram image and then converting the coordinates of the color position in accordance with the scale of the CCT diagram axes. It was assumed that CCT diagram consists of zones defined by the beginning and end of ferrite transformation, the beginning of pearlite transformation, the end of bainite transformation, and the beginning and end of martensite transformation. When developing a predictive mathematical model, an optimization algorithm was used to find a model with the best hyperparameters among classical machine learning models (k-Nearest Neighbors, Support Vector Machine, Linear/Logistic Regression) and based on decision trees (LightGBM, CatBoost). The model solves regression (temperature prediction) and classification (binary mask prediction) problems. The superimposition of a binary mask on the temperature vector made it possible to constrain the resulting phase transformation curve along the time axis. To build test CCT diagrams, a number of dilatometric studies of four steel grades were carried out. The new predictive approach made it possible to achieve satisfactory values of metrics on test CCT diagrams. The average absolute error did not exceed 20°C; the coefficient of determination was in the range of 0.55–0.86, but for the martensite transformation it took negative values, which can be explained by the initial approximation of the transformation by a polygonal chain; ROC AUC metric was at least 0.80.

Key words: continuous cooling transformation diagram, phase transformations, machine learning, regression, classification, dilatometry.
DOI: 10.17580/cisisr.2024.02.07

1. Introduction

Production of rolled products with specified properties is carried out using controlled rolling technology, which includes three main phases: the roughing stage with austenite grain refinement due to deformation in the mill, followed by cooling below the recrystallization temperature with subsequent deformation of the resulting grain, introducing the maximum number of defects into the metal structure. These defects act as nuclei for new grains during the next phase – cooling of the rolled product, resulting in a fine-grained structure with a specific phase composition (ferrite, pearlite, bainite, martensite).

In the development of rolling technology, it is necessary to determine the critical points of steel — the recrystallization temperature, the Chernov points (A_1, A_3), as well as the temperatures at the start of phase transformations, for which continuous cooling transformation (CCT) diagrams are used. CCT diagrams serve as a guide when choosing the cooling schedule (selection of the start and end cooling temperatures and cooling rate). Despite known drawbacks, the main one being the constant cooling rate, which is not maintained during the actual rolling process [1].

The construction of CCT diagrams is carried out on dilatometers and involves the need to prepare samples, conduct tests, and significant labor costs for laboratory assistants in interpreting the results obtained. Moreover, modern rolling mills to produce a single steel grade may use up to thirty variants (depending on the requirements) of chemical compositions, differing in alloying concepts, which necessitates constructing a CCT diagram for each one. The development of machine learning, along with the accumulated data set from published works on CCT diagrams, enables research to develop models for predicting CCT diagrams based on chemical composition.

Initial approaches to the analytical description of CCT curves involved linear equations with variables in the form of the chemical element content. The main limitation of this approach is the narrow range of chemical element content in which it provides satisfactory results. For example, in the study [2], the values of coefficients of empirical equations were selected based on the least squares method for the CCT diagram obtained from the experiment.

Modern machine learning methods and models allow to discover new implicit and complex nonlinear dependencies in the data that improves modeling results. In the studies [3, 4] different solutions for prediction of material phase composition based on neural networks and classical models are represented as well as the economic benefits of their implementation.

In the study [5], the Long-Short-Term Memory (LSTM) architecture was used for phase transformation predictions. It was noted that this architecture is suitable for solving the problem since the curve of an individual transformation is a function of time (this architecture is developed for time series prediction [6]) and shows satisfactory results. The work predicted the percentage of phases depending on the selected cooling rate, with an average error of no more than 10 %.

The research [7] demonstrates the possibility of using fully connected neural networks to predict isothermal transformation curves for nickel-aluminum alloys, showing higher accuracy compared to existing analytical methods.

In the study [8], a higher accuracy of the gradient boosting model was demonstrated in predicting the start of ferrite transformation for carbon steels compared to the "JMatPro" program and decision tree methods.

In the study [9], researchers used an individual model for each curve of the start and end of transformations, also applying the gradient boosting method and obtaining satisfactory accuracy within ±20 °C over a wide range of varying element content. This paper demonstrates the application of gradient boosting models for predicting transformation curves using a combination of regression tasks to calculate the transformation start temperature and classification tasks to determine the boundaries of the corresponding transformation.

2. Methods

2.1. Problem Statement

The variety of possible phases complicates data collection and the formation of the final dataset. Therefore, it was assumed that the CCT diagram consists of the curves presented in **Table 1**, as information on these curves is the most common.

Table 1. Designation and Description of Transformations

Transformation	Transformation Description
F_S	Start of Ferrite Transformation
F_F	End of Ferrite Transformation
P_S	Start of Pearlite Transformation
B_F	End of Bainite Transformation
M_S	Start of Martensite Transformation
M_F	End of Martensite Transformation

For each phase transformation curve, an individual function was sought that links a set of input features to the phase transformation temperature vector. Let X be the input feature matrix with dimensions $n \times m$, where n is the number of observations; m is the number of input features. Then, it is necessary to find a function f such that $f(X) = \vartheta$, where ϑ is the phase transformation temperature vector with dimensions r and $r \leq n$. The temperature range is $(0, \infty)$.

The prediction of the phase transformation curve was carried out by solving two tasks: regression and binary classification. The solution to the regression task is the phase transformation temperature vector:

$$f_r(X) = \vartheta \quad (1)$$

where f_r is the regressor; X is the matrix of input features; ϑ is the temperature vector, with each component corresponding to an observation from X.

The solution to the binary classification task is a binary mask:

$$f_c(X) = mask_\vartheta \quad (2)$$

where f_c is the classifier; X – is the matrix of input features; $mask_\vartheta$ is a vector consisting of zeros and ones, with each component corresponding to an observation from X.

The desired vector of predicted phase transformation temperature values is obtained by the Hadamard product of the temperature vector and the binary mask:

$$f_r(X) \cdot f_c(X) = \vartheta \cdot mask_\vartheta \quad (3)$$

Zero values of the components of the obtained vector are excluded from the final solution. A visualization of the application of the mask followed by the exclusion of zero values is shown in **Fig. 1**.

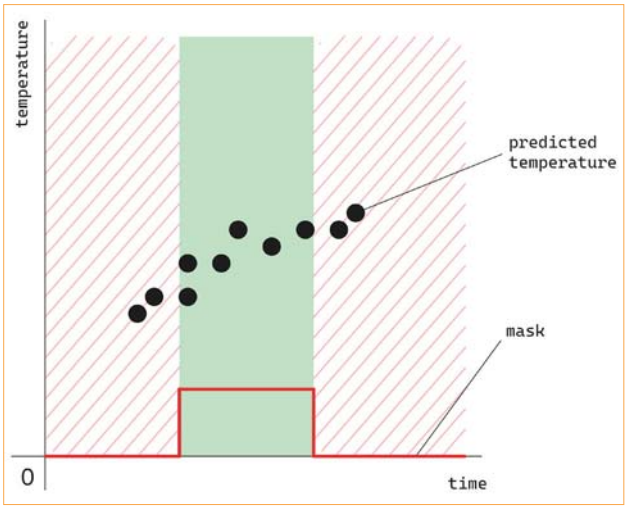

Fig. 1. Visualization of Regression and Classification Composition

2.2. Machine Learning Models

As regressors, both classical models (k-Nearest Neighbors, Support Vector Machine) and gradient boosting with decision trees were used. The best accuracy when working with tabular data is shown by gradient boosting methods like CatBoost, which is based on symmetric decision trees [10] and LightGBM [11]. Logistic regression was used as the binary classifier.

2.3. Metrics

The accuracy of the regression task was evaluated using three quality metrics: Mean Absolute Error (*MAE*), Mean Squared Error (*MSE*) and Coefficient of Determination (R^2).

The *MAE* metric shows the mean absolute error between the predicted and expected temperature values:

$$MAE = \frac{1}{n}\sum_{i=0}^{n-1} | y_i - t_i | \quad (4)$$

where n is the dimension of the vectors y and t; y and t are vectors of predicted and expected values.

The *MSE* metric shows the mean squared error between the predicted and expected temperature values:

$$MSE = \frac{1}{n}\sum_{i=0}^{n-1} | y_i - t_i |^2 \quad (5)$$

The R^2 metric shows the generalization ability of the model. The higher the value of this metric, the closer the predicted values are to the expected ones compared to the mean of all expected values:

$$R^2 = 1 - \frac{MSE}{Var[t]} \quad (6)$$

where $Var[t]$ is the variance of the values in vector .

For classification, both classes were considered equally important. Therefore, the classification metric chosen was the area under the ROC (Receiver Operating Characteristic) curve. The ROC is a set of points (FPR, TPR), where TPR is the True Positive Rate; FPR is the False Positive Rate:

$$ROC\ AUC = \int_0^1 TPR\ dFPR \quad (7)$$

2.4. Model Interpretation

One of the most important stages in the development of mathematical models is their interpretation. Interpretation allows us to establish how much influence each input feature has on the result.

For models based on decision trees, features used at the top of the tree affect the final prediction for a larger proportion of training objects than features that appear at deeper levels. However, there are generalized interpretation methods, such as Permutation Feature Importance and SHAP [12]. This method was used in current study.

2.5. Machine Learning Pipeline

For each phase transformation, the optimal regressor and classifier were searched for. For ease of varying hyperparameters, a pipeline (a sequence of actions on the original data) was used. Each pipeline consisted of a preprocessing stage of the input feature matrix and a subsequent interaction stage with the main predictor. Preprocessing included automatic filling of missing values and data scaling if the predictor's performance strongly depended on data distribution (k-Nearest Neighbors, Support Vector Machine, linear/logistic regression).

The search for the optimal pipeline was conducted using a grid search for hyperparameters with cross-validation (GridSearchCV). In the case of the main predictor (regressor), the pipeline's hyperparameters included not only the hyperparameters of the main predictor but also the predictor itself.

2.6. Digitization and Preprocessing Method

To create the dataset, a digitization method was used, in which the developed program recognizes the pre-labeled curves (**Fig. 2**) and then scales the data.

The labeled diagram is converted into a pixel matrix using the Image.open method from the Pillow library [13], where each pixel is a vector with components whose values correspond to RGB colors. Each phase transformation curve is assigned a specific color: F_S: #e03131; F_F : #1971c2; P_S: #6741d9; B_F: #2f9e44; M_S: #f08c00; M_F: #0c8599.

After digitization, the data needs to be scaled. First, all data is mapped to a range from 0 to 1. Then, the x-axis values are mapped to the range $[x_{min}, x_{max}]$, and the y-axis values to the range $[y_{min}, y_{max}]$. In this case: $x_{min} = 0.1$, $x_{max} = 10000$, $y_{min} = 0$, $y_{max} = 1200$. It was also considered that the horizontal axis has a logarithmic scale.

2.7. Feature Engineering

The final fields of the dataset are presented in **Table 2**. In the study [14] when predicting bainite and ferrite phase transformations, various empirical equations were used as additional features. It was shown that the best results were obtained by adding the Chernov points and a constant value

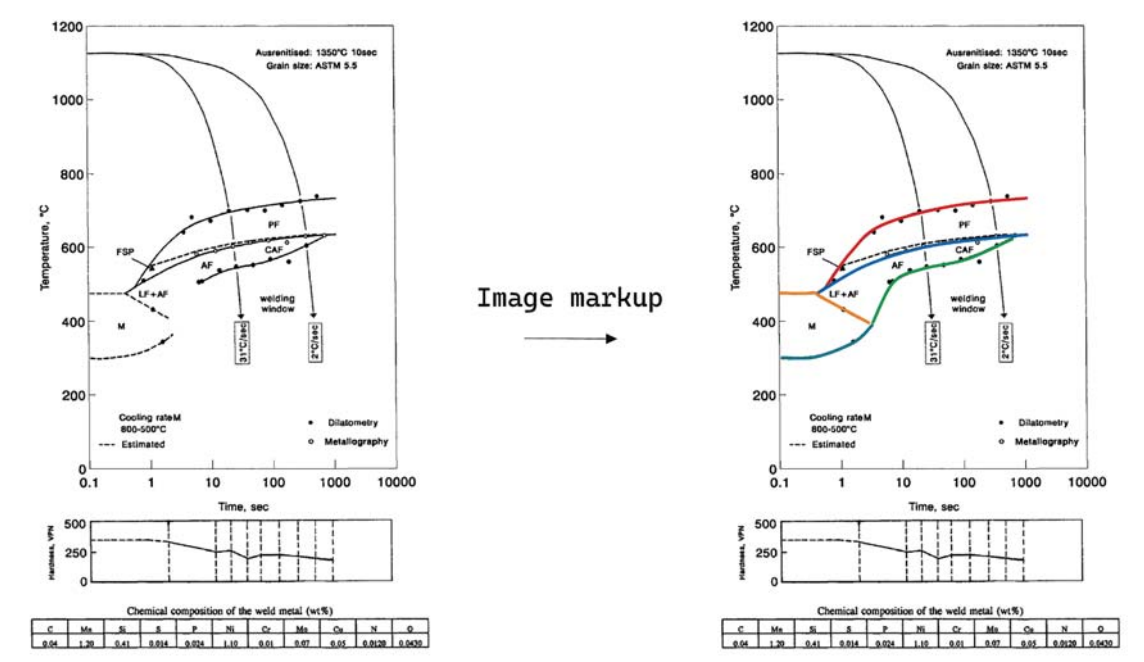

Fig. 2. Image Markup

Table 2. Designation, Description and Measurement Unit of Features

Feature	Feature Measurement Unit	Feature Description
diagram	–	Unique Diagram Name in the Dataset
phase	–	Phase Transformation
CR	°C / s	Cooling Rate
T_{CR}	°C	Start Temperature of Cooling
T_{start}	°C	Actual Start Temperature of Cooling
T_{aust}	°C	Austenitization Temperature
t_{aust}	s	Soaking Time
ε	%	Total Deformation at the Start of Cooling
τ	s	Time at the Point
ϑ	°C	Temperature at the Point
A_1	°C	First Chernov Point during Heating
A_3	°C	Third Chernov Point during Heating
$T_{BSstart}$	°C	Constant Value for the Start of Bainite Transformation
C, Si, Mn, P, S, Cr, Ni, Cu,N, Al, Nb, V, Ti, Mo, B	%	–

for the start of the bainite transformation depending on the chemical composition. Adding new features that characterize the physical properties of the process will improve the accuracy of the modeling results.

To build the dataset, a set of values CR was generated within the range $10^{-1} \le CR \le 10^4$. The values are distributed uniformly according to a logarithmic scale, with 10 values in each decade. Each pair (T_{start} CR) corresponds to a cooling curve, and for each such curve, the intersection points (τ ϑ) with the curves of the digitized diagram are obtained.

First Chernov Point:

$$A_1 = 742 - 29C - 14Mn + 13Si + 16Cr - 17Ni - 16Mo + 45V + 36Cu \quad (8)$$

Third Chernov Point:

$$A_1 = 902 - 255C - 11Mn + 19Si - 5Cr - 20Ni + 13Mo + 55V \quad (9)$$

Constant Value for the Start of Bainite Transformation:

$$T_{Bstart} = 630 - 45Mn - 35Si - 30Cr - 20Ni - 258Mo - 40V \quad (10)$$

3. Results and Discussion

3.1. Data Collection and Analysis

The final dataset for training and testing was formed from digitized CCT diagrams taken from open literature sources [15–21]. The statistics of the dataset are shown in **Table 3**.

Target features depend on each other nonlinearly; therefore, instead of the correlation coefficient, the Chi-square coefficient [22] can be used to analyze their relationships (**Table 4**).

Based on the analysis of the phik-matrixes, the following hypotheses can be formulated. The start temperature of the ferrite transformation is similarly dependent on almost all features except for the cooling start temperature and phosphorus content, which have a greater influence. The greatest influence on the end temperature of the ferrite transformation is exerted by the concentration of silicon and the value of the first Chernov point. For the start of the pearlite transformation, the situation is similar to the start of the ferrite transformation, but manganese is the most important factor.

Table 3. Features Overall Information

Feature	Mean	Median	Minimum	Maximum	Standard Deviation
T_{start}	867.90	850.00	770.00	1350.00	74.89
T_{aust}	1039.09	1100.00	800.00	1350.00	132.77
t_{aust}	186.36	90.00	0.00	1200.00	244.70
ε	25.04	0.00	0.00	50.00	32.99
A_1	734.45	728.34	684.60	931.67	28.38
A_3	857.77	867.56	744.54	895.00	30.23
$T_{BSstart}$	520.14	541.58	228.77	595.16	67.03
C	0.139	0.075	0.036	0.300	0.118
Si	0.301	0.260	0.120	0.940	0.140
Mn	1.294	1.330	0.200	2.020	0.750
P	0.007	0.007	0.001	0.020	0.004
S	0.003	0.002	0.001	0.030	0.004
Cr	0.558	0.110	0.000	2.200	1.472
Ni	0.110	0.075	0.000	0.790	0.155
Cu	0.103	0.110	0.000	0.350	0.089
N	0.004	0.005	0.000	0.013	0.003
Al	0.034	0.027	0.000	0.510	0.058
Nb	0.031	0.030	0.000	0.081	0.026
V	0.021	0.001	0.000	0.260	0.039
Ti	0.009	0.005	0.000	0.037	0.010
Mo	0.083	0.004	0.000	1.040	0.162
B	0.000	0.000	0.000	0.006	0.001

Table 4. Phik-matrix values of Temperature Feature for F_s

Feature	Chi-square coefficient	Feature	Chi-square coefficient
CR	0.54	*S*	0.29
T_{CR}	0.53	*Cr*	0.18
T_{aust}	0.39	*Ni*	0.32
t_{aust}	0.42	*Cu*	0.32
ε	0.31	*N*	0.24
A_1	0.29	*Al*	0.25
A_3	0.27	*Nb*	0.35
$T_{BSstart}$	0.24	*V*	0.27
C	0.40	*Ti*	0.33
Si	0.36	*Mo*	0.18
Mn	0.47	*B*	0.35
P	0.36		

For the end of the bainite transformation, the dependencies are similar to those for the ferrite transformation. The martensite transformation is characterized by dependencies on new introduced features, the initial state of the material before cooling, and carbon concentrations.

3.2. Baseline Model Results

For the baseline model, classical models were chosen for the regressor (k-Nearest Neighbors, Support Vector Machine, and linear regression with L_2 – regularization). The k-Nearest Neighbors model showed the best metric values, which, however, were not satisfactory (mean metric value: $MAE - 35$ °C; $R^2 - 0.34$; $ROC\ AUC - 0.92$).

The baseline model was interpreted using the SHAP method (**Fig. 3**). The figure shows the dependence of SHAP values on the features (the larger the absolute value of SHAP, the higher the contribution of the feature to the calculation of the target feature; the sign of the SHAP value indicates whether the feature value shifts the target feature value positively or negatively).

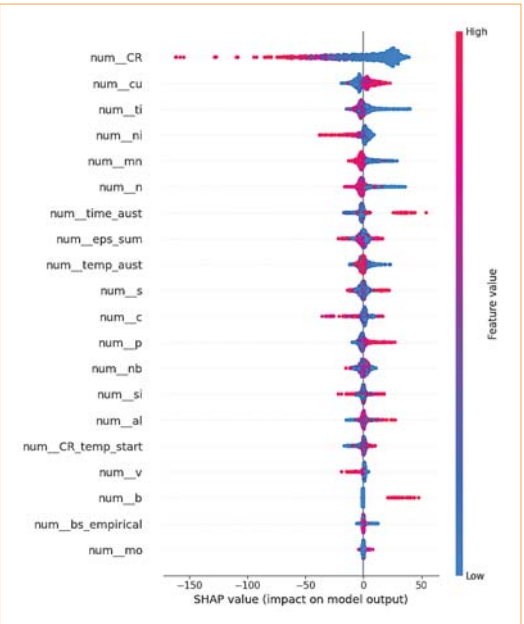

Fig. 3. SHAP Values for F_S

All transformations, except for martensite, are significantly dependent on the cooling rate, with higher cooling rates reducing the transformation temperature. For ferrite and bainite end transformations, an increase in copper concentration shifts the transformation curves upwards on the CCT diagram. Carbon concentration has a substantial impact on the end of the ferrite and the start of the pearlite transformations, shifting the transformation curves downwards on the CCT diagram as the feature value increases. The martensite transformation is characterized by dependence on initial cooling conditions (austenitization temperature, soaking time before cooling, preliminary deformation). Overall, only basic dependencies representing phase transformation processes were obtained by classical models.

3.3. Gradient Boosting Models Results and Verification

After modeling with classical models, decision tree-based models were used: Decision Trees, LightGBM, and CatBoost. The LightGBM library showed the best results. The CatBoost library showed similar results on the training set, but on the validation set, metrics were up to 20 % worse, which may indicate a tendency to overfit even though the depth of the trees was limited to low values. The least accurate were the Decision Trees models, with an average error of more than 40 °C. Metric results for the LightGBM-based model are provided in **Table 5**. The most accurate results were achieved for the start of the martensite transformation and the start of the pearlite transformation. The largest errors were for the end of the bainite transformation (10.5 °C and 13.1 °C) and the start of the ferrite transformation (7.1 °C and 9.2 °C). For the martensite transformation, a low metric value with high accuracy in other cases can be observed, which can be explained by the shape of the transformation curve, which typically represents a horizontal line and is therefore best described by a single value (mean value). The hyperparameters of the LightGBM model with best metric values are shown in **Table 6**.

For LGBM model and ferrite start temperature prediction the most important features are cooling rate, calculated A_3 temperature, *Si* content, austenitization temperature *C* and *Mn* content (**Fig. 4**). For ferrite finish temperature it is

Table 5. Metrics of LightGBM Models (Regression and Classification)

Transformation	Sample	*MAE*	R^2	*ROC AUC*
F_S	Train	9.20	0.86	0.99
	Test	15.70	0.72	0.96
F_F	Train	4.81	0.75	0.99
	Test	18.00	0.42	0.95
P_S	Train	3.68	0.67	0.99
	Test	15.66	0.65	0.94
B_F	Train	13.13	0.53	0.99
	Test	22.30	0.55	0.96
M_S	Train	1.20	-5.01	0.99
	Test	10.30	-2.20	0.80
M_F	Train	4.06	-6.54	0.99
	Test	17.60	-1.90	0.78

Table 6. Hyperparameters of LightGBM Model (F_S, F_F, P_S, B_F, M_S, M_F)

Hyperparameter	Hyperparameter Description	Hyperparameter Value
num_{leaves}	Max number of leaves in one tree	15, 8, 12, 15, 15, 12
reg_{alpha}	l_1-regularization parameter	0.05, 0.1, 0.05, 0.05, 0.1, 0.1
depth	Value of tree depth	10, 6, 10, 6, 6, 8

cooling rate, *C* and *Mn* content and calculated transformation temperatures. For perlite transformation most important are similar to those for ferrite finish plus *Ti*, *Ni* content. For bainite transformation these are cooling rate, calculated transformation temperatures, *Mn*, *Nb*, *C*, *V* content. Finally, for martensite transformation most important features are cooling rate, calculated transformation temperatures and *C*, *Mo*, *Cr* concentration. As can be seen from the description above, LGBM model got dependencies corresponding to known facts from literature.

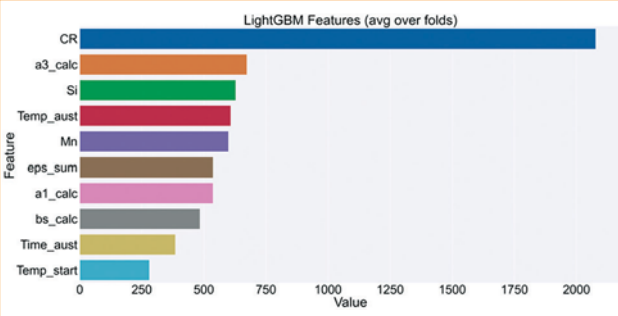

Fig. 4. LGBM model feature importances for F_S

To demonstrate the adequacy of the prediction results, dilatometric experiments were conducted, followed by the construction of CCT diagrams for samples of steels with the chemical compositions listed in **Table 7**.

The prediction accuracy on the test data and the resulting predicted curves are presented in **Fig. 5**. The most accurate predictions were achieved for the start of the martensite transformation, while the least accurate predictions, similar to the training set, were for the end of the bainite transformation.

Table 7. Chemical Compositions of Steels

Element	Steel_1	Steel_2	Steel_3	Steel_4
C	0.050	0.110	0.060	0.080
Si	0.240	0.380	0.220	0.190
Mn	1.800	1.560	0.680	1.630
S	0.001	0.001	0.001	0.003
P	0.012	0.006	0.006	0.011
Cr	0.060	0.050	0.140	0.010
Ni	0.300	0.020	0.100	0.010
Cu	0.240	0.040	0.150	0.010
Ti	0.020	0.018	0.011	0.012
N	0.004	0.006	0.007	0.007
Al	0.035	0.026	0.023	0.035
Nb	0.030	0.033	0.024	0.081
V	0.000	0.067	0.005	0.000
Mo	0.190	0.002	0.000	0.000

For Steel_3 low content of Mn (close to the lower limit of Mn concentration in whole dataset) lead to an absolute error of about 40 °C in predicting ferrite transformation that could mean that it is needed more data on steels having similar composition. For Steel_2 the classification model for perlite transformation showed an error in defining cooling rates at which this transformation occurs. This could be because in training dataset the majority of steels were high strength low alloy steels (HSLA) that mostly don't have perlite transformation at reasonable cooling rates.

Overall, an accuracy within 20 °C can be considered satisfactory, as this level of error is unlikely to lead to significant deviations in the predicted phase composition of the steel after cooling.

4. Conclusion

1. A new model for predicting CCT diagrams based on regression and binary classification is presented. A dataset for training and testing the model was created using a program developed for digitizing CCT diagrams and subsequent preprocessing of the digitized data. A pipeline used for selecting the optimal regression and classification models is described. The best predictors were found to be models based on gradient boosting (LightGBM).

2. The interpretation of the baseline models revealed that all transformations, except for martensite, are significantly dependent on the cooling rate. Carbon concentration has a greater impact on the end of the ferrite transformation and the beginning of the pearlite transformation compared to other factors. Martensite transformation is characterized by dependence on initial cooling conditions (austenitization temperature, holding time before cooling, and pre-deformation).

3. The model was verified using the results from dilatometric experiments on four types of steel. Analysis of the CCT diagram prediction results showed that all predicted temperature values are within the required ranges (the MAE metric does not exceed 20 °C). However, the R^2 metric showed negative values for the martensite transformation, which can be attributed to the nature of the transformation curve, typically a horizontal line that is best described by a single value (mean value).

Future work may include expanding the range of considered chemical elements and introducing new features, particularly for more accurate description of the material's initial state before cooling (e.g., grain size), as well as applying deep learning models given an expanded dataset.

Funding. The research was conducted within the framework of the Russian Federation's strategic academic leadership program «Priority-2030,» aimed at supporting the development programs of higher education institutions. The scientific project PRIOR/SN/NU/22/SP5/26, titled «Creating Innovative Digital Tools for Applying Applied Artificial Intelligence and Advanced Statistical Analysis of Big Data in Technological Processes of Metallurgical Production», was also part of this initiative.

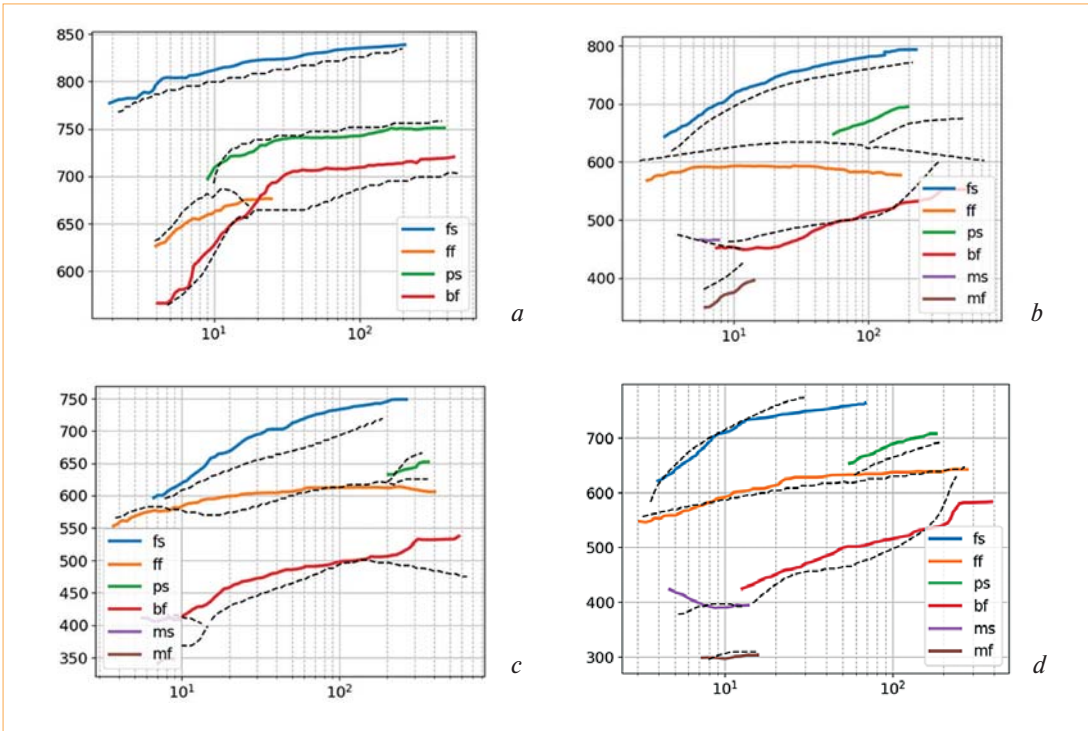

Fig. 5. Comparison of Modeling and Experimental Results: *a* – Steel_1; *b* – Steel_2; *c* – Steel_3; *d* – Steel_4

REFERENCES

1. Efron L. I. Metallovedenie v bolshoi metallurgii. Trubnye stali. Moscow: Metallurgizdat. 2012. 694 p.
2. Ringinen D. A. Formation of a homogeneous structure during thermomechanical treatment under conditions of mill 5000 and stability of impact toughness and cold resistance of pipe steels of strength classes X80 and X100. Dissertation ... of Candidate of Technical Sciences: 05.16.01. Moscow, 2016. 141 p.
3. Zinyagin A. G., Muntin A. V., Tynchenko V. S., Zhikharev P. I., Borisenko N. R., Malashin I. Recurrent Neural Network (RNN) – Based Approach to Predict Mean Flow Stress in Industrial Rolling. *Metals*. 2024. Vol. 14 (12). 1329.
4. Zhikharev P. Y., Muntin A. V., Brayko D. A., Kryuchkova M. O. Artificial Intelligence and Machine Learning In Metallurgy. Part 2. Application Examples. *Metallurgist*. 2024. Vol. 67. pp. 1545–1560.
5. Wróbel J., Kulawik A. Algorithm for determining time series of phase transformations in the solid state using long-short-term memory neural network. *Materials*. 2022. Vol. 15. No. 11. 3792.
6. Lindemann B. et al. A survey on long short-term memory networks for time series prediction. *Procedia CIRP*. 2021. Vol. 99. pp. 650–655.
7. Hernández-Flores L. et al. Determination of TTT Diagrams of Ni–Al Binary Using Neural Networks. *Materials*. 2022. Vol. 15 (24). 8767.
8. Luukkonen J. et al. Gradient Boosted Regression Trees for Modelling Onset of Austenite Decomposition During Cooling of Steels. *Metallurgical and Materials Transactions B*. 2023. Vol. 54. No. 4. pp. 1705–1724.
9. Xiaoxiao G., Wang H., Xue W., Song X., Huang H., Li M., Guang M. Modeling of CCT diagrams for tool steels using different machine learning techniques. *Computational Materials Science*. 2020. Vol. 171. 109235.
10. Ustimenko A., Beliakov A., Prokhorenkova L. Gradient boosting performs gaussian process inference. *arXiv*. 2023. arXiv: 2206.05608.
11. Shi Y., Ke G., Chen Z., Zheng S., Liu. T.-Y. Quantized Training of Gradient Boosting Decision Trees. *Advances in Neural Information Processing Systems*. 2022. pp. 18822–18833.
12. Lundberg S. M., Lee S. I. A unified approach to interpreting model predictions. *CoRR*. 2017. 1705.07874.
13. Lundh F. Pillow. *Pypi.org*. 2024. Available at: https://pypi.org/project/pillow/.
14. Zhang Y. et al. Phase Transformation Temperature Prediction in Steels via Machine Learning. *Materials*. 2024. Vol. 27. No. 5. 1117.
15. Teplukhina I. V., Golod V. M., Tsvetkov A. S. CCT diagram plotting based on the numerical analysis of dilatometric tests results. *Letters on Materials*. 2018. Vol. 8. No. 1. pp. 37–41.
16. Bräutigam–Matus K. et al. Experimental determination of continuous cooling transformation (CCT) diagrams for dual-phase steels from the intercritical temperature range. *Metals*. 2018. Vol. 8. No. 9. p. 674.
17. Grajcar A., Morawiec M., Zalecki W. Austenite decomposition and precipitation behavior of plastically deformed low-Si microalloyed steel. *Metals*. 2018. Vol. 8. No. 12. 1028.
18. Schindler I. et al. Effects of austenitization temperature and predeformation on CCT diagrams of 23MnNiCrMo5-3 steel. *Materials*. 2020. No. 13 (22). 5116.
19. Zurutuza I. et al. Effect of Quenching Strategy and Nb-Mo Additions on Phase Transformations and Quenchability of High-Strength Boron Steels. *JOM*. 2021. Vol. 73. pp. 3158–3168.
20. Krbata M. et al. Austenite decomposition of a lean medium Mn steel suitable for quenching and partitioning process: comparison of CCT and DCCT diagram and their microstructural changes. *Materials*. 2022. Vol. 15. No. 5. 1753.
21. Wang Z. et al. Effect of tungsten addition on continuous cooling transformation and precipitation behavior of a high titanium microalloyed steel. *Metals*. 2022. Vol. 12 (10). 1649.
22. Baak M., Koopman R., Snoek H., Klous S. A new correlation coefficient between categorical, ordinal and interval variables with Pearson characteristics. *Computational Statistics & Data Analysis*. 2020. Vol. 152. 107043.